On the Modelling of Macrosegregation during Twin-Roll Casting

IOP Conf. Series: Materials Science and Engineering **529** (2019) 012041 doi:10.1088/1757-899X/529/1/012041

On the Modelling of Macrosegregation during Twin-Roll Casting

C M G Rodrigues[1], A Ludwig[1], A Kharicha[1,2], M Wu[1] and A Vakhrushev[2]

[1] Department Metallurgy, Montanuniversitaet Leoben, Leoben, Austria
[2] Christian Doppler Laboratory for Metallurgical Applications of Magnetohydrodynamics, Montanuniversitaet Leoben, Leoben, Austria

christian.gomes-rodrigues@unileoben.ac.at

Abstract. Solidification during twin-roll casting happens by cooling of the melt between two counter-rotating rolls, where the molten alloy is constantly fed in. For an inoculated Al-melt, grain growth leads to a gradual increase of solid fraction, so that a coherent solid network forms. Depending on the process condition, this solid network might be subjected to compression within the gap between the two rolls. By using a two-phase volume average model that accounts for (i) transport and growth of spherical grains within a flowing melt, (ii) formation of a coherent solid network above a specific solid fraction and (iii) viscoplastic flow of the solid network saturated with interstitial melt during casting and compression, the process is numerically analysed. It is found that an optimum process with minimum macrosegregation can be achieved for conditions where the kissing point of the two viscoplastic semi-solid shells nearly coincides with the roll nip. It is demonstrated how casting speed, cooling intensity and strand thickness must be related to hit the optimum process window.

1. Introduction

Twin-roll casting is an emerging commercial material processing technique that produces thin strips directly from molten metal. As the casting and hot rolling processes are performed at the same time in the production line, the technology requires less initial investment and ensures a more energy efficient process than conventional continuous casting techniques.

As a result, interest has grown among engineers and researchers, and many studies have been carried out over the past years. For instance, several experiments have been conducted to optimize the operating conditions, such as the pouring temperature, set-back distance, strip thickness or casting speed [1,2]. Other researchers have instead studied micro- and macro-defects, ranging from surface bleeds, internal defects, hot tearing and buckling [3,4]. However, there is obviously a limit to how much information one can obtain solely from measurement techniques applied to experimental trials.

Comprehension of the twin-roll casting process requires a thorough understanding of the complex flow dynamics that develop during the production of the strip. That is why numerical models have been employed to accomplish this task. Accordingly, due to the stiff nature of the problem, finite element simulations are widely used for that purpose, although they often rely on a single phase thermo-mechanical model originally designed for the analysis of pure rolling [5].

However, deformation of the partly solid shells is usually an important mechanism in twin-roll casting. It is known that the deformation of a solid-liquid mixture above a certain solid fraction can

lead to macrosegregation [6,7]. In order to capture these flow dynamics, it is essential that the solid-liquid mixture is considered as a contiguous solid skeleton saturated with interstitial liquid when the solid fraction exceeds the specific threshold. In the present paper, this stage is referred to as the viscoplastic regime and the major distinction – compared to the lower solid fraction regime – is that the rheology of the flow is now dictated fundamentally by the solid phase. Therefore, in the case of an alloy in the semi-solid state being subjected to deformation, the corresponding motion of the coherent structure drives the liquid flow, which means that at this stage, the mechanical character of the process takes over the fluid flow dynamics, and consequently, the melt becomes the passive phase which reacts to the solid behavior.

In the present work, a two-phase volume-average model is used to replicate a twin-roll casting scenario. The model considers the entire spectrum of solid fractions, and so it is able to deal with an almost completely molten alloy and turn it into a fully solid material, and vice-versa. Furthermore, above a specific criterion, the equiaxed crystals are assumed to behave according to a dense coherent network which interacts with the interstitial liquid. This means that mush deformation is accounted for by mean of a viscoplastic model that is employed when the solid fraction is above 0.57.

2. Numerical implementation

The simulation of the twin-roll continuous casting presented in this paper relies on a two-phase Eulerian-Eulerian volume-average model. The general approach solves mass, momentum, species, and enthalpy conservation equations for each phase. Additionally, a transport equation is also taken into account for the calculation of the number density of grains across the domain. A detailed description of the corresponding governing equations has been made in a previous publication [8], so the interested reader can refer to those contributions for further details. For the sake of conciseness, only the most relevant equations will be highlighted here.

The important novelty of this model is the implementation of the viscoplastic regime, which is imposed when the solid fraction exceeds g_s^t = 0.57. The change in material behavior is transmitted through the viscous stress tensor, which is then defined differently depending on the solid fraction.

$$g_s \boldsymbol{\tau}_s^{eff} = \begin{cases} 2 g_s \mu_s \mathrm{dev}\left(\dot{\boldsymbol{\varepsilon}}_s\right) & \text{for } g_s \le g_s^t \\ 2\frac{\mu_s^{\mathrm{app}}}{A}\mathrm{dev}\left(\dot{\boldsymbol{\varepsilon}}_s\right) + \mu_s^{\mathrm{app}}\left(\frac{1}{9B}\right)\mathrm{tr}(\dot{\boldsymbol{\varepsilon}}_s)\mathbf{I} & \text{for } g_s > g_s^t \end{cases} \quad (1)$$

Below the viscoplastic threshold, the equation is defined by the general Newtonian viscous stress tensor (assuming that bulk viscosity is zero). This expression is analogous to the one adopted in the liquid phase with the strain rate tensor for either of the phases (*i*) being given by $\dot{\boldsymbol{\varepsilon}}_i = 1/2\left(\nabla \mathbf{v}_i + (\nabla \mathbf{v}_i)^T\right)$. In the viscoplastic regime, on the other hand, experimental studies on the behavior of metallic alloys at high temperatures show that the solid phase can be described by the equation presented above [6].

Comparison between the two equations defined for each regime shows that above the transition criterion a second term is considered in the formulation. This term is related to the bulk viscosity and corresponds to a normal compression force considered in this regime. Note that A and B are two rheological parameters proposed by Nguyen et al. [6], which can be written as follows:

$$A = \frac{3}{g_s^{6.47}} \quad \text{and} \quad B = \frac{1}{g_s^{6.94}} - 1 \quad (2)$$

In Eq. (1), the terms μ_s and μ_s^{app} represent the solid viscosities in each of the regimes. For low solid fractions, Ishii [9] postulated that the mixture viscosity of a set of particles can be expressed

according to the power-law viscosity model. Assuming the general mixture rule as $\mu_{mix} = g_s\mu_s + g_l\mu_l$, the solid viscosity can be given by:

$$\mu_s = \frac{\mu_\ell}{g_s}\left(\left(1-\frac{g_s}{g_s^p}\right)^{-2.5g_s^p} - (1-g_s)\right) \tag{3}$$

where g_s^p is considered as a fitting constant that represents the random loose packing limit for spheres. Following the experimental results from Olmedilla et al. [10] $g_s^p = 0.585$ has been adopted here.

Regarding the viscoplastic regime, the apparent solid viscosity generally accepted in the literature takes the form of the Herschel–Bulkley model:

$$\mu_s^{\text{app}} = 3K_v\left(\sqrt{3}\dot{\varepsilon}_s^{\text{eq}}\right)^{m-1} \tag{4}$$

where K_v and m are the viscoplastic consistency and the strain-rate sensitivity, respectively. The latter parameter is usually assumed as a fixed value which depends on the material properties. In the present work, it is set as 0.213. On the other hand, the viscoplastic consistency can be calculated by combining the strain-rate tensor proposed by Nguyen et al. [6] and the Norton-Hoff stress-strain-rate relation. It takes the value of 6.31×10^6 Pa s.

As for the equivalent strain rate presented in Eq. (4), it is given by the following expression:

$$\dot{\varepsilon}_s^{\text{eq}} = \sqrt{\tfrac{2}{A}(\dot{\boldsymbol{\varepsilon}}_s : \dot{\boldsymbol{\varepsilon}}_s) - \left(\tfrac{2}{3A} - \tfrac{1}{9B}\right)\text{tr}(\dot{\boldsymbol{\varepsilon}}_s)^2} \tag{5}$$

which again depends on the rheological parameters defined in Eq. (2).

Details on the microscopic phenomena and the coupling between the conservation equations have been described in detail in companion papers [7,8].

3. Results and discussion

The schematic diagram of the geometry replicated in the simulations is illustrated in Fig. 1. The results have been obtained for an inoculated Al-4wt.%Cu alloy ($\cong 2.5$wt.%). Since the width of the sheet is in concept much larger than its thickness, the test case is assumed to be 2D. A mesh composed of 5700 cells was used, which corresponds to an average cell size of approximately 0.85 mm per 0.47 mm. The time step was variable, but stayed in the order of 10^{-4} s a few moments after the start of the simulation. Also, the effect of gravity is neglected at this point, so the interpretation of the results is not influenced by the sedimentation of the crystals. The densities of the solid and liquid phases are assumed to be equal (ρ=2743 kg/m^3), so solidification-induced feeding is also neglected at this point.

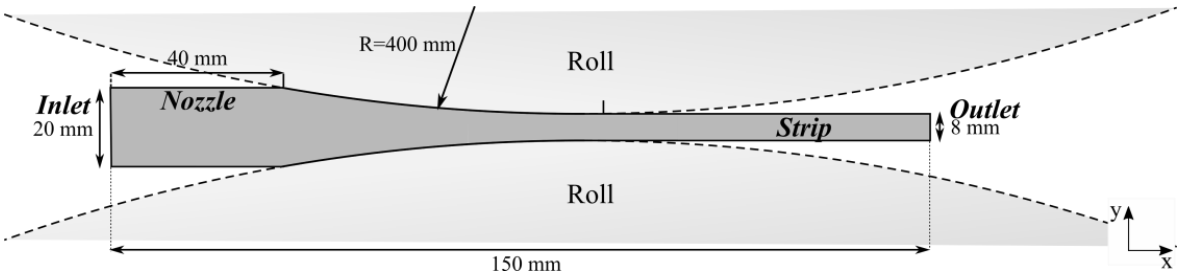

Figure 1. Schematic representation of the twin-roll continuous casting process.

The melt is injected into the domain through the inlet with a fixed pressure field (p=10^5 Pa) at 925 K. Dirichlet boundary conditions are imposed at the inlet to solid fraction (10^{-5}, i.e., almost negligible amount), initial crystal diameter (d=5 μm), and liquid and solid species mass fractions (c_l=0.025 and c_s=0.0036, with the values taken from the phase diagram). Regarding the temperature, it is set as 925 K at the nozzle surface, and zero gradient at the outlet. In the roll and strip sections, on the other hand, a heat flux is imposed between the surface and each of the two phases with a constant heat transfer coefficient of 5.5 kW/m^3/K. Even though the assumption of equal heat transfer coefficient in the strip and roll is generally not precise in practical environments, it has been adopted in the present work to simplify the simulation as much as possible for a proper understanding of the flow dynamics and macrosegregation patterns.

The velocity boundary conditions for the liquid phase are assumed as free-slip at the nozzle, roll and strip sections, whereas for the solid phase they are set as no-slip instead. At the outlet, two different scenarios are considered: Case A has a casting speed of 0.040 m/s, whereas Case B is set with a casting speed of 0.025 m/s.

The steady state results for the solid fraction in both Case A and Case B are illustrated in Fig. 2 a) and b), respectively. The black contour line in each of the snapshots represents the solid fraction at which the viscoplastic regime starts. In Fig. 2b), besides this, also the contour line from Case A is presented with white dots.

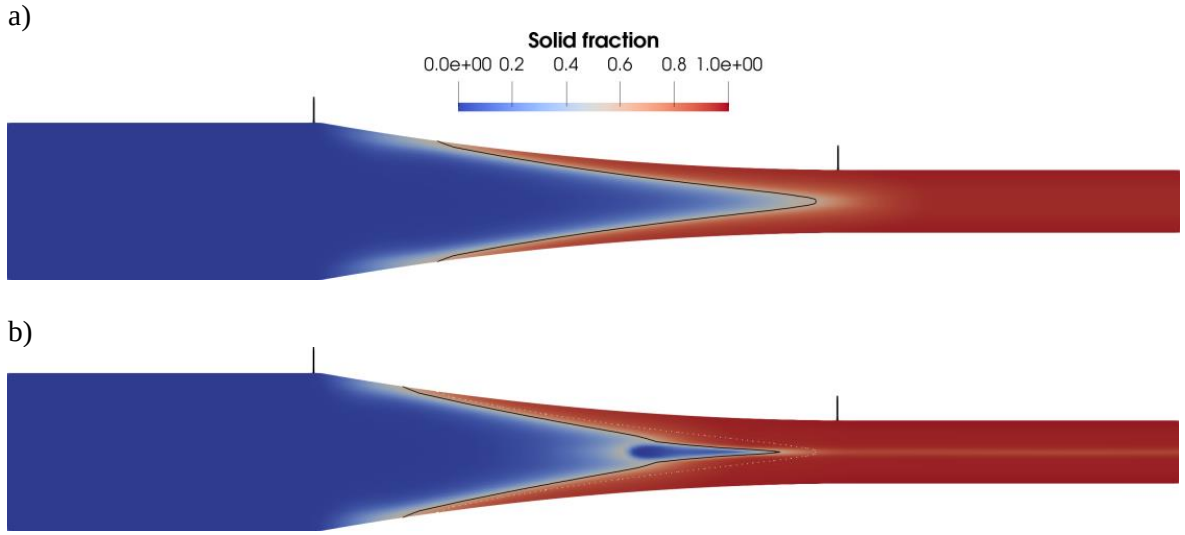

Figure 2. Steady state results for the solid fraction in both a) Case A and b) Case B.

It can be seen that as the casting speed is reduced to 25 mm/s, the cooling rates become higher and thus the thickness of the partly solid shells increases. As a result, the kissing point occurs slightly upstream, which leads to larger compression forces to take place, and thus the viscoplastic mush ends up by squeezing more material out of the structure (in the form of melt and equiaxed crystals) against casting direction (i.e. reverse flow). This causes melting to occur in this particular area and thus solid gradually disappears (see the dark blue area appearing along the centerline upstream of the kissing point).

Obviously, such flow dynamics have an important effect on macrosegregation. Deviations from nominal composition are shown in Fig. 3 for both cases examined here. It becomes clear that in Case B the significant positive segregated centreline appears as a result of the reverse flow discussed above. Furthermore, negatively segregated bands located near the surface are predicted next to positively segregated bands in both Case A and Case B. To understand these findings, one has to combine information regarding the general direction of the flow with the relative velocity between solid and liquid.

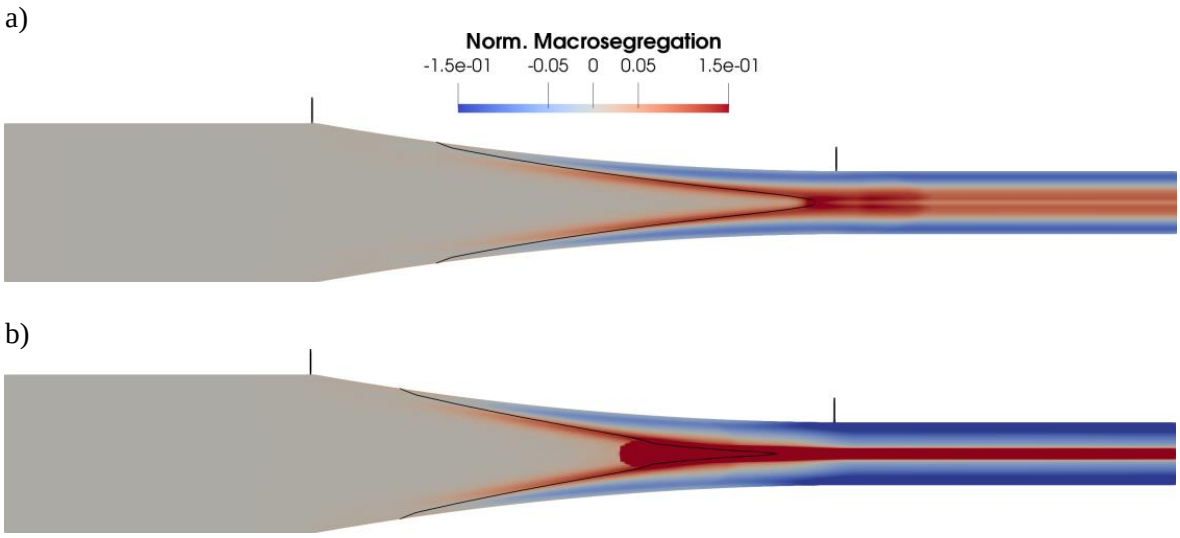

Figure 3. Steady state results for solid fraction in a) Case A and b) Case B. Data range has been limited for better understanding of the deviations from nominal composition.

Figure 4 presents the relative velocity between solid and liquid in x- (top half) and y-components (bottom half) with black arrows representing the relative velocity of the flow. Note that the arrows only express the direction of the relative flow and not the magnitude as the arrows have all the same size. Instead, the magnitude of the relative flow between phases can be identified through the relative velocity snapshots. The arrows, on the other hand, allow one to keep a clear perception of the dominant phase in each region of the domain. Also, note that the range of the color legend has been reduced so the different mechanisms become clearer.

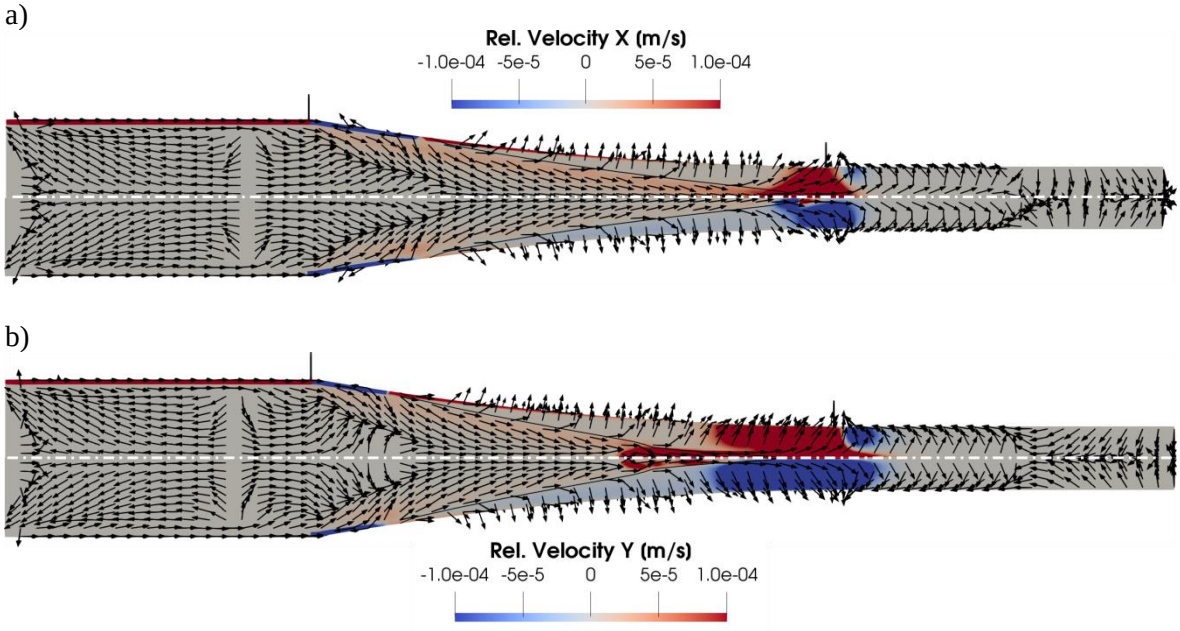

Figure 4. Steady state results of liquid velocity for both both x- (top half) and y-component (bottom half) for a) Case A and b) Case B. Arrows representing the relative velocity between solid and liquid phases are shown on top of the relative velocity snapshots.

The change in relative velocity at the walls is obviously due to the different boundary conditions imposed to both phases, as described in the previous chapter. Then, in the section of the domain where the rolls are being enforced (between the two vertical markers), one can notice in both cases a slight reddish area appearing in the non-viscoplastic regime that fades away as we move towards the centreline of the domain. This corresponds to an area where the solid phase is faster than the liquid both inwards and downstream. This is because the abrupt decrease in velocity of the melt (between casting speed near the surface to almost zero velocity along the centreline) is not accompanied immediately by the solid phase because of the much higher viscosity.

Notice that right after the contour line which establishes the transition to the viscoplastic regime, the arrows start pointing outward instead of inward in both Fig. 4 a) and b). This finding marks the start of the viscoplastic regime, and means that (contrary to the previous state) the liquid is now moving inwards faster than the solid. It also correlates well with the negative macrosegregation bands shown in Fig. 3, near the surface. It can be explained by a compression-induced expulsion mechanism occurring due to hot rolling of the solid-liquid mixture, which causes segregated melt to be squeezed out of the viscoplastic skeleton. As a result of these occurrences, the enriched melt travels to adjacent regions in the domain, causing positive macrosegregation to develop in those regions. This justifies the appearance of bands with positive deviation from nominal composition located next to bands with negative deviation in Fig. 3 a) and b).

At the kissing point, the two semi-solid shells merge together and form a single continuous casting strip. Comparison between Case A (Fig. 4 a) and Case B (Fig. 4 b) shows that in the latter, the relative velocities in both components are much bigger in this region because of the larger compression forces, as discussed above. In the region where the reverse flow develops in Case B, melt is moving upstream faster than the solid, which means that the compression-induced expulsion is such that interstitial liquid is squeezed out against casting direction. On the other hand, after the two solid shells have merged together, the blue area in the y-component and red area in the x-component of the velocity mean that the liquid is moving faster than the solid inwards (because of compression-induced expulsion) and upstream (because it is easy for the flow to travel through lower viscosity regions). Such flow dynamic leads to an increase in positive macrosegregation near the kissing point region, while inducing a slight negative macrosegregation along the centreline because the enriched melt there is moving upstream (arrows are horizontal along centreline).

4. Conclusion

Even though twin-roll casting is a promising processing technique, the material properties depend greatly on the operation parameters (e.g. casting speed, strip thickness and casting temperature), which in turn are difficult to control. In the present paper, two different casting speeds are presented, and the outcome of the simulations are discussed in terms of macrosegregation. The two cases illustrate significant casting speed differences, and the corresponding effect on the quality of the strip.

The present results show that, for a specific strip thickness, there is a corresponding casting speed that provides minimal deviation from nominal composition. Below this threshold, further cooling of the semi-solid is enforced which eventually increases the strength of the compression-induced expulsion mechanism and amplifies macrosegregation.

Acknowledgments

This work was financially supported by the FWF Austrian Science Fund (P28785-N34) which the authors gratefully acknowledge.

References

[1] Zhang X M, Jiang Z Y, Yang L M, Liu X H, Wang G D and Tieu A K 2007 Modelling of coupling flow and temperature fields in molten pool during twin-roll strip casting process *J. Mater. Process. Technol.* **187**–**188** 339–43

[2] Sahoo S, Kumar A, Dhindaw B K and Ghosh S 2012 Modeling and experimental validation of

rapid cooling and solidification during high-speed twin-roll strip casting of Al-33 wt pct Cu *Metall. Mater. Trans. B Process Metall. Mater. Process. Sci.* **43** 915–24
[3] Jin I, Morris L R and Hunt J D 1982 Centerline Segregation *J. Met.* 70–5
[4] Lockyer S A, Yun M, Hunt J D and Edmonds D V. 1996 Micro- and macrodefects in thin sheet twin-roll cast aluminum alloys *Mater. Charact.* **37** 301–10
[5] Lee Y S, Kim H W, Cho J H and Chun S H 2017 Coupled thermal-fluid-mechanics analysis of twin roll casting of A7075 aluminum alloy *Met. Mater. Int.* **23** 923–9
[6] Nguyen T G, Favier D and Suery M 1994 Theoretical and experimental study of the isothermal mechanical behaviour of alloys in the semi-solid state *Int. J. Plast.* **10** 663–93
[7] Rodrigues C M G, Ludwig A, Wu M, Kharicha A and Vakhrushev A 2019 A Comprehensive Analysis of Macrosegregation Formation during Twin-Roll Casting *Metall and Materi Trans B* 1–17 https://doi.org/10.1007/s11663-019-01527-x
[8] Ludwig A and Wu M 2002 Modeling of globular equiaxed solidification with a two-phase approach *Metall. Mater. Trans. A* **33** 3673–83
[9] Ishii M 1977 *One-Dimensional Drift Flux Model and Constitutive Equations for Relative Motion Between Phases in Various Two-Phase Flow Regimes*
[10] Olmedilla A, Založnik M and Combeau H 2017 DEM simulation of dendritic grain random packing: application to metal alloy solidification *EPJ Web Conf.* **140**